Texture Evolution of Aluminum Alloy AA5750 by Simulated Accumulative Roll Bonding

Sanjev Sharma
Associate Professor
Department of Mechanical Engineering, [1]Amity University , Gurgaon, India

Abstract : The accumulative roll bonding technique is one of the well-known severe plastic deformation process to achieve sheet material with nanostructures and high strength. The properties of such sheets vary a lot from those of usually rolled sheets. It is hence popular to have a simulation construction that can perfectly calculate the material properties, as well as the developing texture and anisotropy through the process. In this paper, we put forward such a framework for multiple pass rolling using explicit finite elements and implanting the visco-plastic self-consistent (VPSC) polycrystalline texture model for the material response. To smooth the progress of multiple pass rolling, we plan a new solution mapping method which transfers the material properties from the plastically deformed finite element mesh to a new property of the material. as well as, a two-level parallelization plan with the decomposition of the finite element domain by means of message passing interface (MPI) and thread based parallelization of the material retort using open MP to make certain compact simulation times. The analytical capabilities of the planned framework are established by simulating the accumulative roll bonding of aluminum alloy AA5750 sheets. The simulations validate the working of the solution mapping scheme, and clearly show the development of a through-thickness gradient of texture and anisotropy in the roll-bonded sheet after two passes.

Keywords– Nono structured material, Accumulative roll bonding, Visco plastic self-consistent, solution variables mapping, Finite elemen multi-level parallelization.

I. Introduction

The acceptance of new materials in the engineering sectors hinges continually more and more on the possibility to reliably model their mechanical actions through processing and under distinctive usage situation, and their breakdown when subjected to disastrous loading. Material models have thus become a crucial ingredient for the promising discipline of integrated computational materials engineering (ICME), which promises to considerably cut down the materials development system [1].For instance, the integration of computational material models in the product design method and in manufacturing process simulation would permit engineers to search new ways for optimizing the chattels of a component through processing. The main key for successful execution of the ICME paradigm is the accessibility of material models which illustrate the multiple relations among processing, microstructure, properties, and performance in a multiscale modeling framework. Though, several innovative materials or processing methods reliable material models are not till now accessible. In particular, the accumulative roll bonding process to fabricate high strength metal sheets, for engineering applications, would earnings from a trustworthy and forceful material model to optimize the process parameters and express the consequential microstructure and mechanical properties. Along with a variety of Severe Plastic Deformation (SPD) processes, the Accumulative Roll Bonding (ARB) technique is most capable for achieving nanostructure in metallic worksheet material. It has proposed by Saito et al. [2], the ARB technique is based on stacking two metal sheets and after providing for them to a rolling mill where the thickness is reduced by 50%. As the geometrical dimensions of the processed worksheet stay more or less unaffected to the initial material, the process can be simply repeated. Both worksheets are primarily degreased and wire brushed to take away thick oxide layers in the absence of such oxide layers and obsessed by huge plastic strains, the stacked layers combine at the interface to develop good bonding properties. A detailed overview of the principles of ARB-processing and the properties of some processed materials is provided in Ref. [3]. A most important benefit of the ARB technique is that it can be simply incorporated into existing industrial rolling trains without major change and can be scaled up to fabricate worksheet materials with a Nanostructured microstructure on an industrial scale [4]. In addition, the ARB technique occurs several potentials to tailor materials properties by producing malty layered worksheet materials [5, 6, 7,8,9, 10] or reinforced composite sheet materials[11, 12, 13].The repeated roll bonding of the sheets in the ARB technique leads to large accumulation of plastic deformation resulting in a Nano-microstructure. This nano microstructure causes a major increase by almost a factor of two or three in the strength of the material, in evaluation to the coarse-grained counterpart. Although this is usually set by a drop off in ductility, it has newly been reported that function of ARB to low-density sheet materials, like aluminum alloys, can produce in both high strength and high ductility of the material [5] and has been credited to room temperature strain rate sensitivity of the material [14,15,16]. The ARB technique itself involves a large number of parameters, like rolling speed, friction between the rolls and the feedstock, number of rolling passes, stacking and rolling direction etc., which can have a substantial result on the properties of the roll bonded worksheet. Although similar to a conventional rolling process in principle, the role of such process parameters is either considerably improved or entirely different in ARB due to the high thickness reduction and repeated stacking of roll bonded sheets in every pass. For example, sheared surface layers due to friction between the rolls and the feedstock give rise to a characteristic through thickness strain gradient in the roll bonded sheet. With repeated cutting and stacking, the shear profile changes considerably [14], leading to different rates of microstructure development along the thickness of the worksheet. As a result, the number of rolling passes has a visible effect on the thickness strain gradient. The anisotropy in the roll bonded sheet is thus not just a function of texture/microstructure, but also the strain gradient and the number of rolling passes [17]. It is hence to be likely that the properties of ARB worksheets vary appreciably from those of conventionally rolled sheets [18], and additionally, can significantly impact the further application of the roll bonded sheet. Since the mentioned aspects, it is attractive to have a computational framework to simulate and recognize the ARB process in order to attain optimized process parameters, so as to stay away from trial-and-error experimental setups. To date, most studies on ARB processed materials have been experimental investigations to understand both the process and the enhanced properties of the roll bonded sheet, as evident in the references mentioned above. By contrast, few computational studies can be found in the literature; these studies have been limited to understanding individual aspects of the ARB process. For instance, texture evolution which plays an important role during ARB has been the subject of a few numerical investigations. Heason & Prangnell [19] performed EBSD and

X-ray measurements on a roll bonded AA1100 sheet, and analyzed the evolution of texture using the Taylor [20] full constraints model with simple and idealized textures. A similar study was performed on AA3003 by Pirgazi et al. [21], but by using the ALAMEL model [22]. In contrast to the idealized deformation paths assumed in the previous two studies, Li et al. [23] used realistic strain histories to investigate the texture evolution in commercially pure aluminum by means of the ALAMEL model. Finite element (FE) simulations of a single-pass rolling process were employed to obtain the relevant strain histories; the FE simulations were calibrated to embedded pin experiments in order to reasonably estimate the shear deformation [24] seen in ARB processed materials. A primary goal of this work is to establish a computational framework that enables the simulation of multiple pass ARB processes, whilst simultaneously accounting for the change in texture and anisotropy of the material. The principal idea here is to obtain the structural response using an FE calculation, whilst the material response is obtained by \averaging" the constitutive behavior of individual crystals in a dened3polycrystal. Such \averaging", termed generally as numerical homogenization, is now a well-established technique to solve problems involving the micro-mechanical behavior of polycrystalline materials. An excellent review of such methods is provided in Ref. [25]. Although different factors of such a multi-scale framework are available, all boil down essentially to two choices: a) the polycrystal homogenization theory to be used [26], i.e. full field or mean-eld theory, and b) implementation of the macroscopic model within the multi-scale analysis framework [22], i.e. whether the polycrystalline model is to be embedded in the FE computation, or merely used in a hierarchical fashion. Polycrystal homogenization theories can be broadly classified into two categories, viz. full-eld and mean-eld methods. Full field methods provide a fairly accurate assessment of the intragranular stress and strain fields. Examples of such methods include the crystal plasticity finite element method (CPFEM)and crystal plasticity fast Fourier transform (CPFFT) method. CPFEM has been extensively used with artificial microstructures (e.g. [27, 28, 29] as well as experimental microstructures obtained typically from EBSD measurements (e.g. [30, 31, 32]. The CPFFT method ([33, 34] is identical to CPFEM with one major difference -the governing equations are solved in the Fourier space. Although restricted to periodic microstructures in principle, a major advantage of CPFFT over CPFEM is the speed of computation [35].The choice of such full eld methods for numerical homogenization, however, necessitates the usage of FE2-type methods (e.g. [36]), which would essentially result in lengthy computation times for multiple pass ARB simulations. In what concerns the implementation of the numerical homogenization model within the multi-scale analyses is framework [22], choice must be made between embedding the model in the FE computation | i.e. interrogating the polycrystalline model during each increment | and using it in a hierarchical fashion [37, 38], where the parameters for a macro-scale (anisotropic) phenomenological yield criterion (e.g. [39], [40]) are pre-computed by interrogating the polycrystal model. This choice, as a result, is clearly a decision on balancing accuracy and speed, since embedded models tend to be more accurate but less efficient (in terms of computational times) than hierarchical models. Nonetheless, it must be noted that adaptive sampling strategies (e.g. [41]) can be used in conjunction with embedded models to achieve results in shorter lead times. The fundamentals of our computational framework lie in the aforementioned multi-scale approach; we use a mean-field homogenization model embedded in an FE computation. In particular, we use the visco-plastic self-consistent (VPSC) model of Lebensohn & Tolle [42] as our choice of the mean field model, since it has been widely used for many studies involving both cubics (e.g. [43]) and hcp (e.g. [44], [45], [46]) materials and is known to provide fairly accurate predictions of the texture and anisotropy [47, 48]. The VPSC model is embedded in an explicit finite element framework using the commercialize element software Abaqus. It must be pointed out that this embedded VPSC-FE model is not entirely new, and has been the subject4of previous studies (e.g. [44], [49], [50]). However, such basic implementations are insignificant to overcome the challenges posed by the ARB process. A primary challenge in simulating the ARB process -as seen from the discussion before -is the increase in the number of elements, by a factor of two, with each ARB pass. Additionally, due to the large thickness reduction in each rolling pass, distortion of the FE mesh is a further problem that needs to be tackled. In view of this, we propose a novel solution mapping scheme that helps map the texture, grain shape and other relevant material state variables from the deformed mesh to a new mesh, thus alleviating the distortion related problems. Also, since the mapping can be done to a completely new mesh, it allows us to circumvent the doubling of elements with each pass. Furthermore, we strive to create an implementation that is robust, fast and efficient. This is done by exploiting the factorized interface of the user material routine in Abaqus R by using a multi-level parallelization, i.e. decomposition of the FE domain for the structural response, and parallelization of the material response inside each domain using multiple open MP [51] threads. Additionally, we probe the polycrystal model only periodically, thus ensuring further improvement in simulation times. We point out that notwithstanding the results presented in the current work, the proposed computational framework can be used for the simulation of other forming processes like conventional rolling, deep drawing, etc.

II. ARB SIMULATIONS

The accumulative roll bonding process was simulated using the open MP parallelized VPSC VUMATin combination with the linear elastic update described in section 3.2. The working of the VUMAT was first verified by performing benchmark tests on a single element and loading it in uniaxial tension, uniaxial compression, and simple shear. Comparison of the results with those from the standalone version (ver. 7) of the VPSC code [71] showed identical stress-strain responses and textures, indicating the correctness of the VUMAT implementation. Further tests with multiple elements were performed to ensure the sanity of the parallelized code. These results of these benchmark tests are provided elsewhere [72, 73]. The simulations showed here consist of two rolling passes. To model stacking of sheets before the second pass, the required internal variables were mapped onto a new mesh using the procedure described in section 3.4.4.1. Simulation setup The FE model used for the ARB simulations is shown in fig. 1. The model is set up such that the rolling, transverse and normal directions are parallel to the x, y, and z-axis, respectively. The feedstock consists of two Al5754 sheets, of length 5mm and thickness 1mm, stacked upon each other. The Voce hardening parameters for the material are taken from Ref. [74]. Symmetry conditions are exploited by modeling only one half of the feedstock (i.e. only one of the two Al5754 sheets) in the simulations. The above condition has the consequence that bonding between the two sheets is essentially modeled as \hard" contact, with the bonding of the rolled sheets precluded. The modeled sheet is discredited with 500 hexahedral elements; reduced integration elements (C3D8R) with enhanced stiff
ness hourglass control are used in the simulations. In addition to symmetry, plane strain conditions are imposed in the transverse direction, resulting effectively, in the simulation of a thin slab of material in the center of a fairly wide sheet, as shown in g. 1(b).Such a model provides a more accurate material response for which it is primarily set up, and allows additionally for a relatively fine spatial discretization.

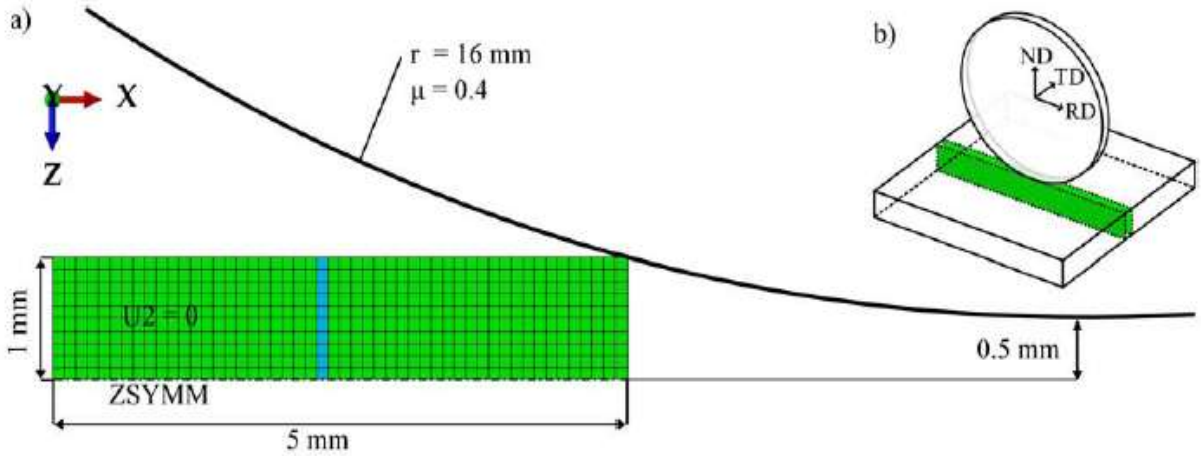

Figure 1: Initial configuration used for simulations of the ARB process. The blue strip indicates the elements for which texture and polycrystal states are saved.

The rollers, modeled as rigid with a diameter of 32mm, rotate at a speed of 80 rpm. Contact between the roller and the feedstock is imposed through anisotropic friction coefficient of = 0:4. Mass scaling is used to artificially increase the stable time increment, whilst taking care to keep the kinetic effects of such a scaling to a minimum. The used stable time increment in the simulations is t = 4x10-6 s. The simulations are carried out in parallel with eight open MP threads but without domain decomposition. For the first rolling pass, all elements in the feedstock are initialized with identical texture comprising 250 spherical grains of random orientation and equal volumes. Texture output, along with additional internal variables (cf. table 2) are requested as so-called End-of-pass data for 10 elements along the cross-section of the feedstock (marked in blue in fig. 1

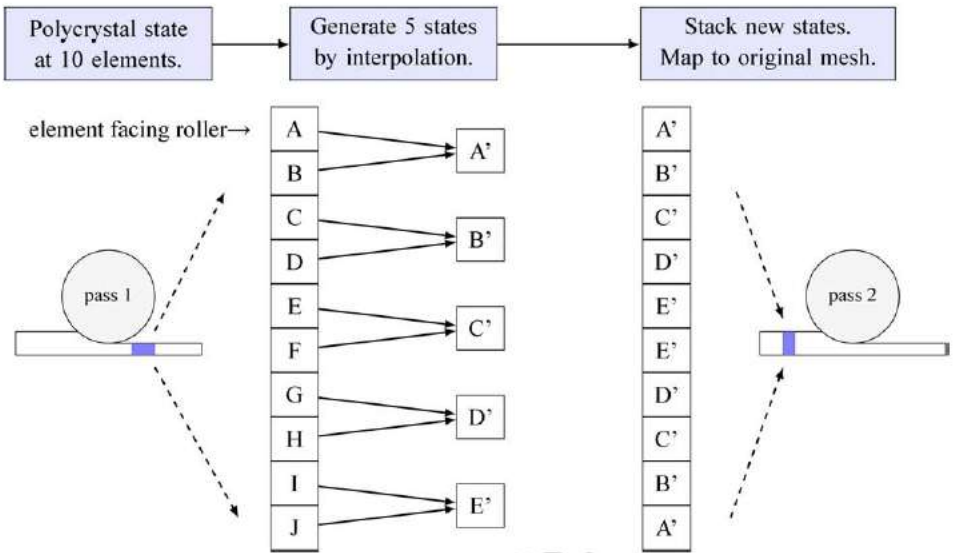

Figure 2 A schematic of the solution mapping scheme that maps the polycrystal state after the first pass on to a new initial mesh for the second pass. Polycrystal states of ten elements marked in blue are mapped onto five elements by interpolating the states of adjacent elements. The mapped solution state is then duplicated in five more elements by assuming refection symmetry. This new stack of ten elements with the mapped solution states is then replicated along the length of the FE mesh used for the subsequent pass.

These elements have been purposefully chosen along the center of feedstock, so as to avoid boundary effects likely to be present around the ends of the roll bonded sheet. For the second rolling pass, the same finite element model is retained. However, the modeled feedstock is now assumed to be a roll bonded sheet obtained from the first rolling pass. To effectively carry over the material state from the first rolling pass to the second, we use the solution mapping procedure described previously in section 3.4. To this end, we use the material state of the ten elements marked in blue in fig. 1. The mapping is done as follows. Since the original thickness of the sheet is 1mm, and the thickness reduction imposed in the first pass is 50%, the z-coordinate (normal direction) of the centroid of all the ten elements (forming the top sheet in the first pass) may be expected to lie between 0mm and 0:5mm. Now five evenly spaced points at 0.05, 0.15, 0.25, 0.35 and 0.45 mm are selected in this interval. If a neighborhood is now established based purely on the z-coordinate, each new element may be considered to be in the vicinity of two polycrystal states of the roll bonded sheet. A new state is then generated for each of the five points by linearly interpolating the two neighbor polycrystal states. This mapping procedure is schematically represented in fig. 2. We note that each vertical slab of 10 elements in the new FE mesh corresponds effectively to 20 polycrystal states (or stacking of two sheets) in the ARB sheet obtained after the first pass. The five newly generated polycrystal states are copied onto the lower set of 5 elements, assuming a mirror symmetric stacking sequence. The state of the polycrystal in this vertical stack of 10 elements is now replicated along the length of the sheet.

In effect, we have now mapped the material state of the deformed FE mesh of the first pass to the undistorted initial mesh of the second pass. It must be pointed out that the use of only polycrystal states for the mapping procedure is a matter of convenience. A more elaborate schema could be envisaged, wherein the End-of-pass data of all elements in the deformed finite element mesh could be used for the mapping procedure, thus resulting in an improved representation of the microstructural inhomogeneity. The use of such an extensive set would, however, necessitate data throughput between individual computation processes and physical memory storage lead to the significant increase in simulation times. With the polycrystal states accounted for, the second rolling pass can be simulated in a straightforward18manner like the first pass. The same process parameters as that of the first pass are retained for the simulation of the second pass.

III. Results

Fig. 3 shows the distribution of von Mises equivalent stresses in the deformed geometry after the stand second rolling pass. Towards either end of the rolled sheet, the deformation is clearly inhomogeneous. However, for a greater part of the sheet around the center, a steady stress distribution is observed. It is exactly in this region that we request the texture and End-of-pass data, in order to obtain a material state that is by and large re effective of the rolled sheet. The ten elements, numbered between 261 and 270, from which the material state is used for the mappingprocedure are also indicated in fig. 3

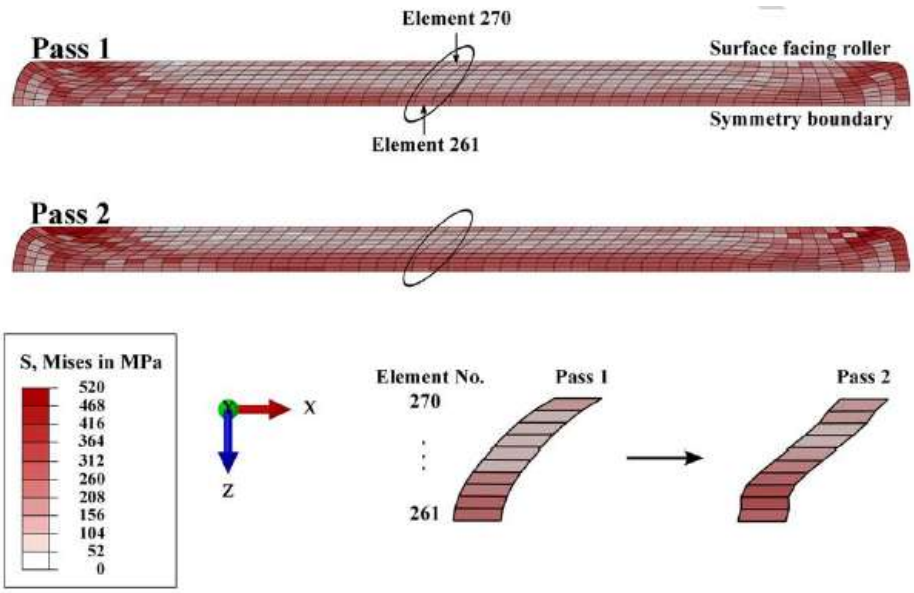

Figure 3: Stress distribution (von Mises equivalent stress) in the rolled sheet after the first and the second pass. A steady distribution can be appreciated in the greater part of the sheet, in which for a stack of ten elements the texture and End-of-pass data are requested as output. The close-up view shows the deformed shape of elements from which output has been requested. In both rolling passes, a through-thickness shear gradient can be clearly observed.

The textures obtained from the aforementioned central stack of elements after the first ARB pass is shown in fig. 4. The pole figures were computed using the Mat lab toolbox MTEX ([75]). A clear gradient in the texture is evident through the thickness of the sheet. The elements towards the center of the sheet exhibit a texture close to typical rolling textures of face-centered cubic (fcc) materials, whilst those towards the surface of the sheet evidence an additional shear component. This can be better understood by looking at g. 5(a) which shows the components of textures in individual elements. Towards the center of the sheet, the texture is dominated by the Sand Brass components, along with considerable contributions of the Copper and Taylor components indicating a strong fcc rolling texture. With increasing distance from the center, the relative volume fraction of these components decreases, whilst that of the rotated cube component increases reacting a texture with significant shear deformation. This dominance of the rotated cube component at the surface of the sheet is noteworthy, particularly due to its relative absence at the center of the sheet. The textures of this central stack of ten elements are then mapped onto the top five elements of the new mesh using the mapping procedure described previously in detail. The mapped textures are presented in fig. 6. Essentially, the textures of two adjacent elements (e.g. 270 and 269, or 268 and 267 in fig. 6) in the thickness of the rolled sheet are then mapped onto a single element (cf. A or B in fig. 6) in the new mesh. Similitude between the mapped textures and the corresponding reference states can be easily appreciated. Indeed the mapped texture, along with additional mapped variables that govern the state produce a mechanical response that lies between those of the reference states. The initial state of the bottom five elements in the new mesh is then obtained by copying the state of the top five elements, albeit by refection, so as to obtain a stacking

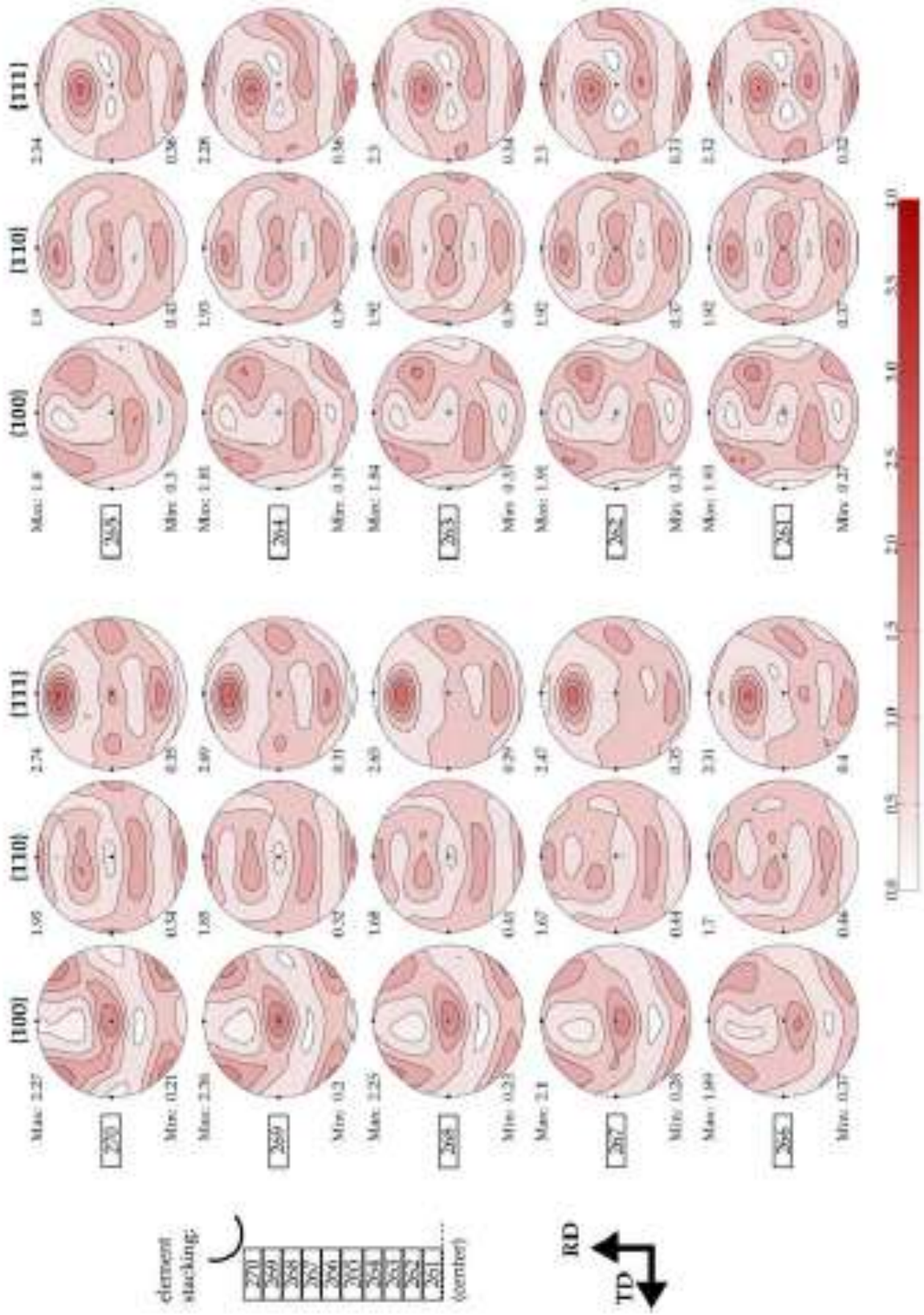

Figure 4 Textures in the central stack of ten elements after rolling pass 1. A through-thickness gradient in texture is evident. Near the sheet surface, the rotated cube component is dominant. Towards the center of the sheet stack, the texture shows typical rolling components.

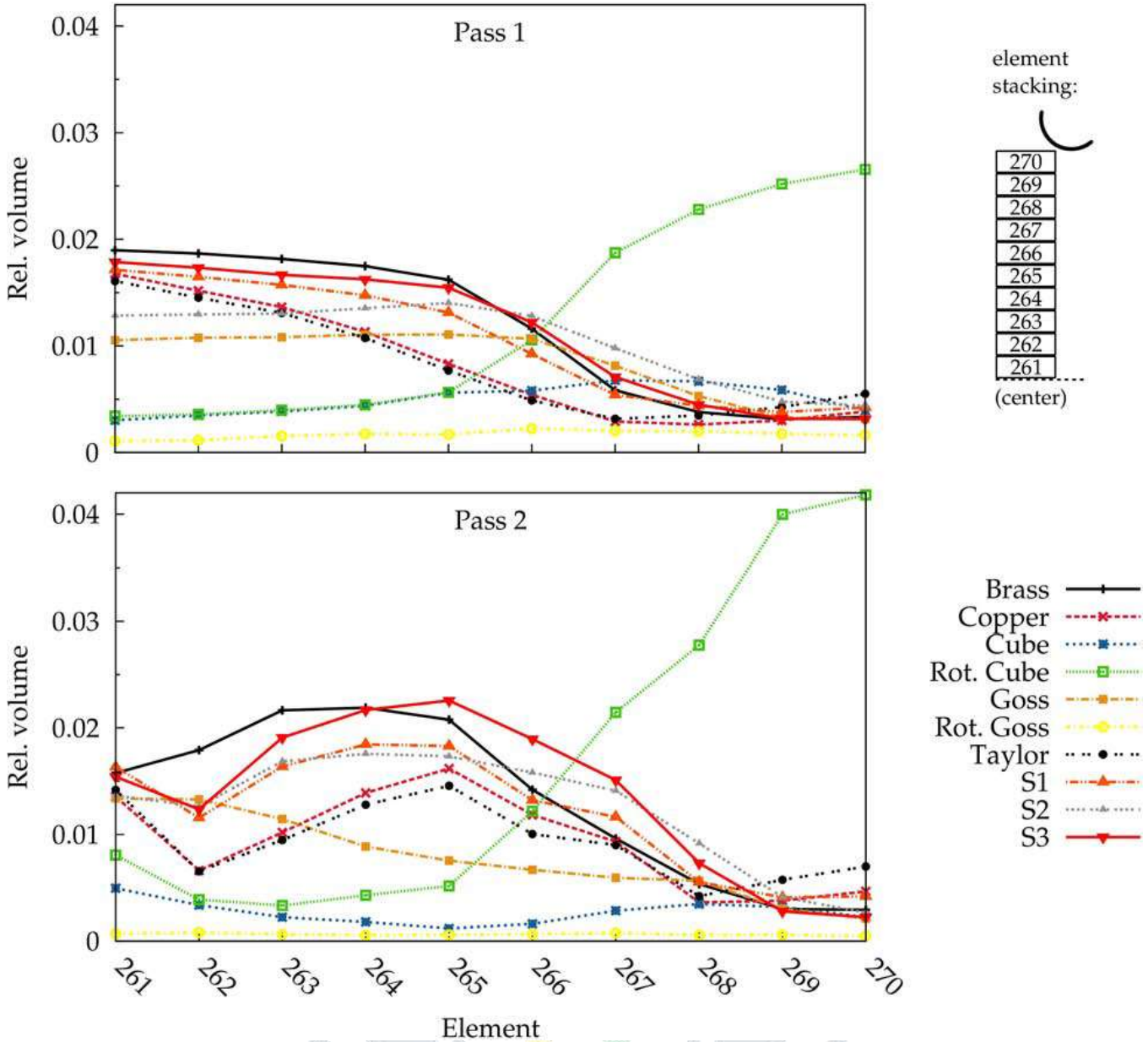

Figure 5: Texture components in the central stack of ten elements after the first and second rolling pass

sequence Roller-A-B-C-D-E -E-D-C-B-A. Consequently, the top sheet of the feedstock for ARB pass 2 has a shear dominated texture at its surface and a strong rolling texture at its center. In addition to the textures, other variables defining the state of the polycrystal are also mapped on to the top five elements of the new mesh and copied onto the bottom five to obtain the stacking sequence as mentioned above. Of the remaining three solution variables (cf. table 2), the mapping of critical resolved shear stresses and the cumulative shear, which are scalars, is straightforward and is not presented here for the sake of brevity. Mapping of the grain shapes, by contrast, is non-trivial and demands careful scrutiny. Fig. 7 shows the results of the grain shape mapping. The average shape of the polycrystal is initially a sphere and evolves into ellipsoids of varying shapes and orientations in each of the central stacks of ten elements. For demonstration, the ellipsoids of four elements (numbered 261, 261, 269 and 270, and corresponding to two adjacent elements near the center and surface of the top sheet) after the first pass are shown in fig. 7(red ellipsoids). The mapped ellipsoids, shown in green, share a strong resemblance to the reference states in terms of not just the shape, but also the orientation. This clearly indicates the soundness of the mapping procedure. The mapped ellipsoids are then used as the initial average shape of the polycrystal for the second rolling pass. For completeness, the final shape of the two ellipsoids after the second pass is also shown in g. 7. We note that for the second pass, further simulation parameters from the first pass are retained. Symmetry boundary conditions are once again exploited to reduce the size of the simulated domain. This inevitably leads to rolling of two sheets, where the properties of the bottom sheet are mirror symmetric to those of the top sheet. For the current scenario, where the process involves roll bonding of two sheets of the same material, this does not make a difference. However, for the simulation of roll bonding of laminates, symmetry boundary conditions must be used with caution. The textures after the second rolling pass are presented in fig. 8, with the volume fractions of different texture components plotted in fig. 5(b). The output is again requested in the central stack of elements, as in the first pass. Similar to the first pass, elements close to the sheet surface show a texture with a considerable amount of sheer, characterized by a strong rotated cube component. A reduction in the volume fraction of the rotated cube component towards the center of the rolled sheet is simultaneously followed by an increase in the volume fraction of the S and Brass components. However, in contrast to the first pass where a gradual increase of the S-component towards the center of the sheet was seen, a peak around apparently the center of top sheet is seen. We ascribe this to the presence of a strong rolling texture at the center of the roll bonded sheet after the first pass. The gradient observed in the texture of the rolled sheet has considerable influence on the yield behavior of the sheet.

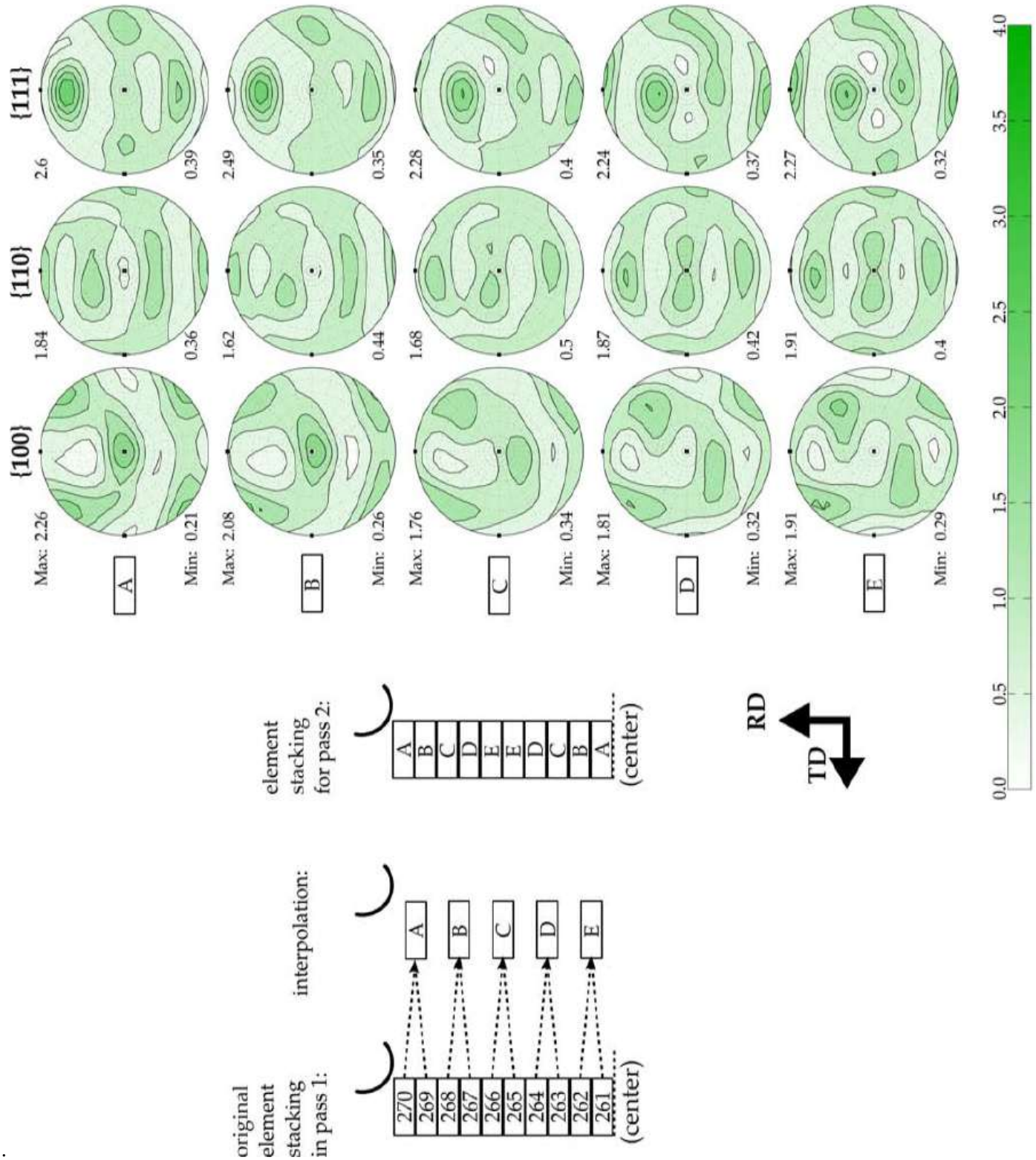

Figure 6: Mapped textures, which serve as input to pass 2. Also shown is a schematic of the mapping between the reference stack of ten elements (numbered) and the top five elements in a stack of ten elements in the new mesh, which are then copied onto the bottom ve elements through rejection. Similitude between the mapped textures and the corresponding reference states from pass 1 (fig. 4) is evident.

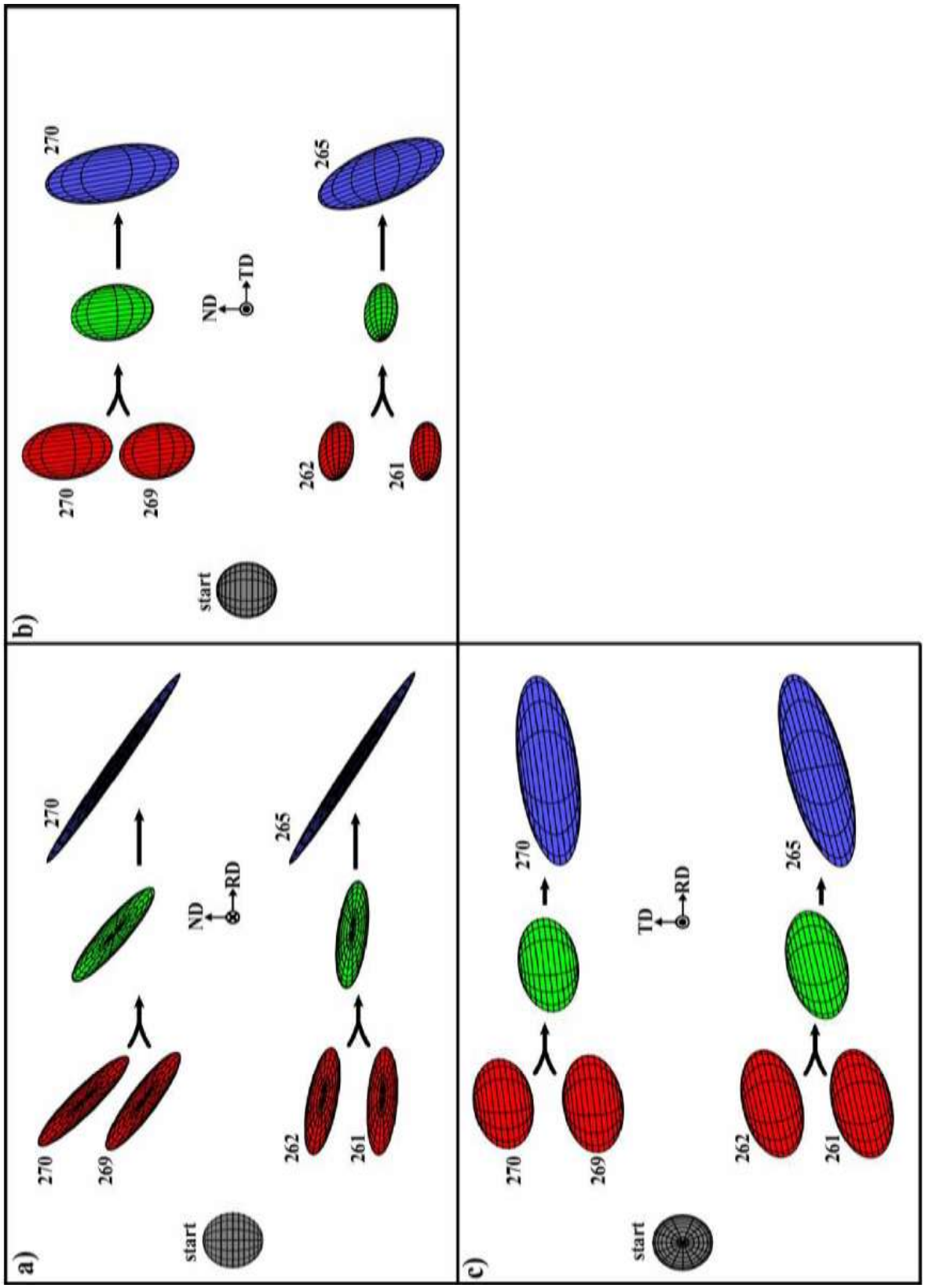

Figure 7: Front (a), side (b) and top (c) views of the average ellipsoids used in the ARB simulations. Gray: common initial grain shape; red: grain shape in elements261, 262, 269 and 270 after the first rolling cycle; green: interpolated grain shapes for starting configuration of elements 265 and 270 in the second rolling pass. The interpolated shape of 265 is based on the shape of element 261 and 262; for the interpolated shape in 270, the reference states are 269 and 270. Blue: shape in elements265 and 270 after the second cycle.

Fig. 9 shows the polycrystal yield surfaces of the central stack of ten elements for which output of the material state was requested. The yield surfaces are projected onto the 11 -22 plane, assuming plane stress conditions (33 = 0). In addition to the yield surfaces after the first and second rolling passes, we also present the initial yield surface (polycrystal with 250 randomly oriented grains) for comparison. The yield surfaces after the first and second rolling passes have been calculated with standalone VPSC by using the texture and End-of-pass polycrystal states of the central stack of ten elements as input. The yield surface of the initial configuration is more or less isotropic, and its shape can be approximately characterized by the von Mises yield criterion.

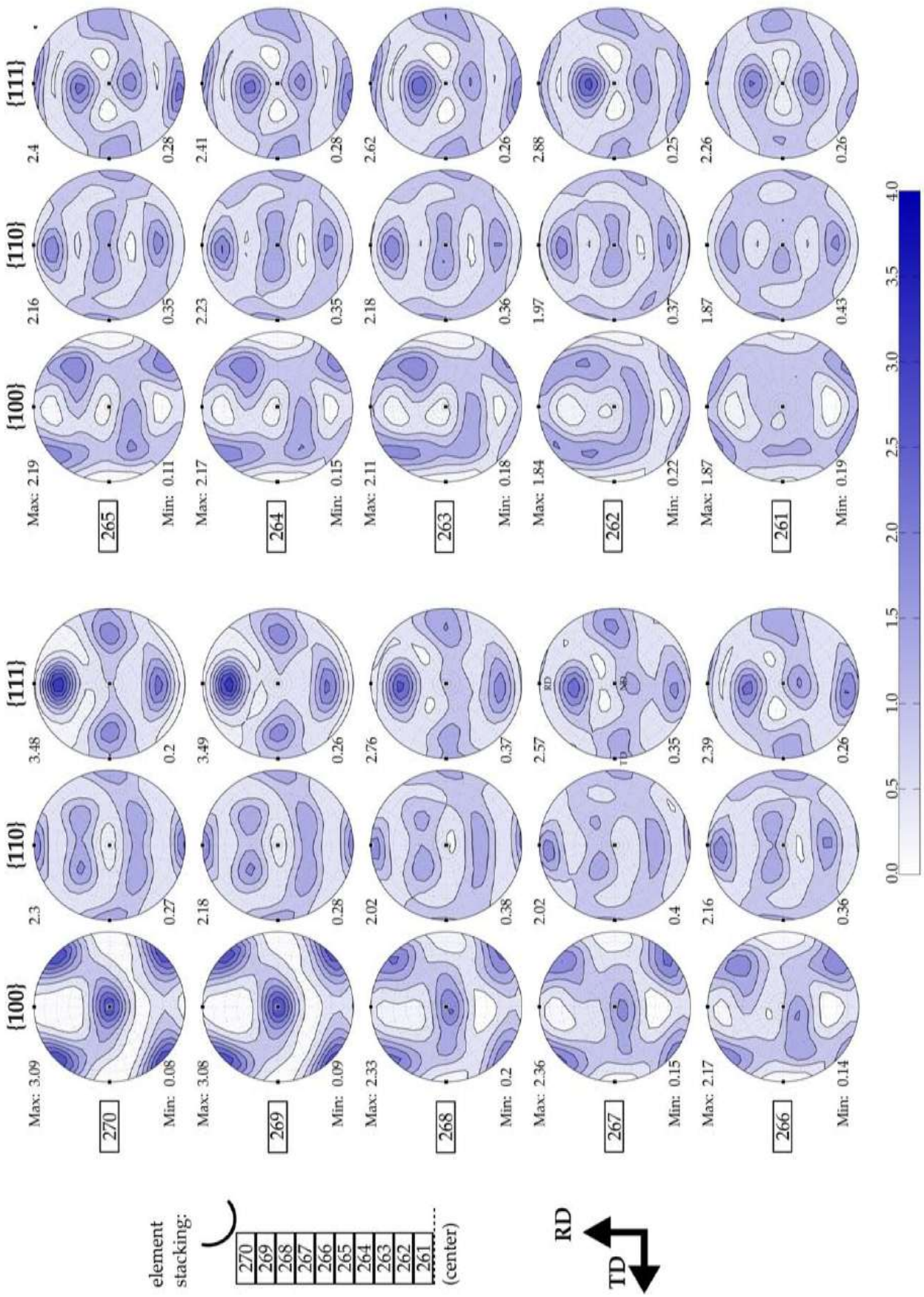

Figure 8: Textures in the central stack of ten elements after rolling pass 2. A through-thickness texture gradient is evident. The rotated cube component dominant near the sheet surface.

Rolling components are formed near the center of the sheet stack, with each rolling pass, isotropic hardening leads to an increase in the size of the yield surface, with a higher hardeningrate in the the yield surfaces are presented in section.

IV. SIMULATIONS WITH A 3D MODEL

A further important aspect of the current work is the usage of multi-level parallelization -domain decomposition using MPI and parallelization of the VUMAT using openMP. To address this issue, we performed full three-dimensional simulations of the ARB process, using different parallelization combinations and a moderately be mesh. The initial and deformed FE models are shown in fig. 10. It is clear

from the stress distribution shown in fig. 10 b that the stress levels reached in the full 3D model are comparable to those in the plane strain rolling simulations, indicating the plausibility of the quasi-2D approach presenters pass than in the second. Noticeably, this isotropic hardening leads to almost no change in the shape of the yield surface in the element close to the center of the rolled sheet and is evidently a consequence of the underlying strong rolling texture. The domination of shear in the elements close to the surface leads to an anisotropic evolution of the shape of the yield surface, and the shape can no longer be characterized by a simple von Mises type of yield criterion.

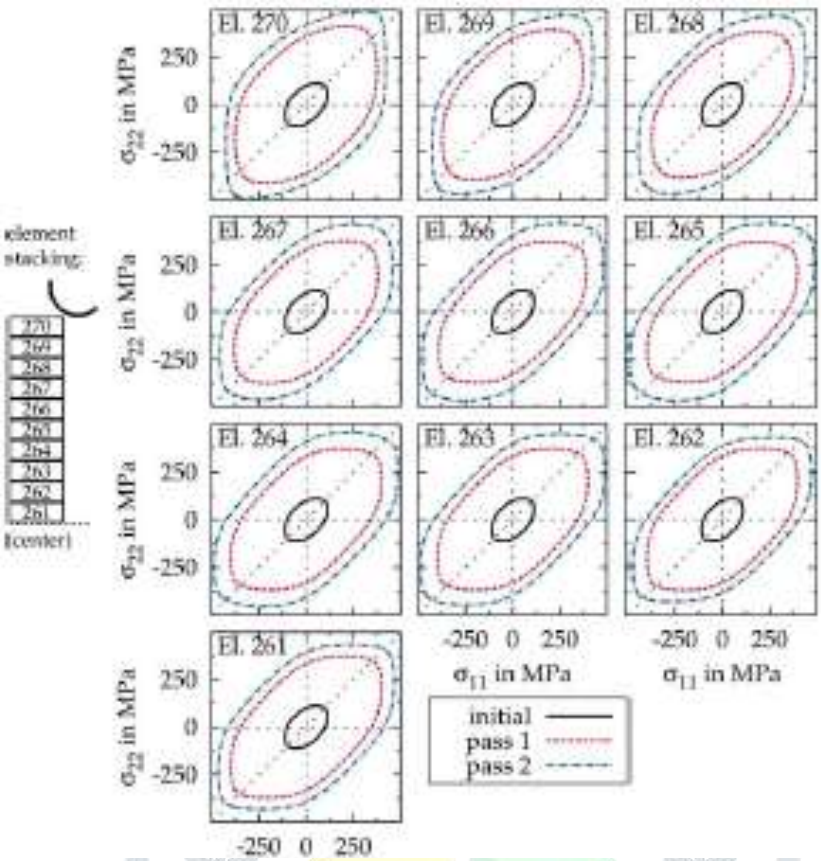

Figure 9: Polycrystalline yield surfaces in an initial state and after ARB pass 1 and 2. Towards the center of the sheet stack and especially in element 261, the yield surface undergoes a more or less isotropic evolution. In the sheet surface, in element 270, anisotropic evolution is observed.

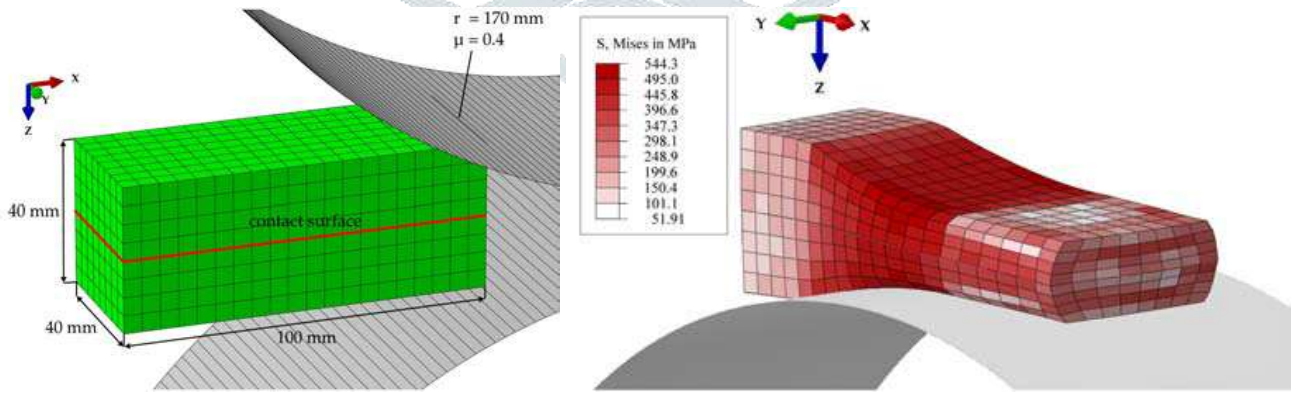

Figure 10: Initial (left) and deformed (right) FE models of the full 3D simulations of the ARB process. The deformed structure shows the von Mises stress state in the material.

in section 4. However, more interesting are the computation times required for these full 3D computations. Assimilation with purely domain decomposition based parallelization that uses 8 domains takes approximately105 hours. By contrast, a simulation using the two-level parallelization, with 2 domains and 4 threads each takes merely 36 hours. Note that in both these simulations
the number of campuses used is essentially the same.

These simulation times unambiguously show the potential for the novel computational framework proposed in the current work. The true advantage of the two-level parallelization is indeed visible in simulations with larger domains where such client amount of work can be parallelized using Open MP threads. The open MP based parallelization has the advantage of improved mitigation of load imbalance that might occur during the simulation of complex processes like ARB. Nonetheless, it must be pointed out that load imbalance is still likely to be

a problem due to the linear update of the constitutive response used in the current work. Recall that this is necessitated by the small stable time increment in Abaqus /Explicit. Consequently, an embedded framework that calls the VPS model in every increment becomes computationally exorbitant with increasing complexity of the FE model. Segurado et al. [49] show that the calculation of the consistent tangent moduli for implicit finite element requires the mere addition of the elastic moduli (C) to the polycrystal tangent moduli (M) obtained from VPSC, necessitating the use of acceleration techniques that call the embedded model only when required. The linear constitutive update is an example of such a technique and can easily lead to load imbalance in the OpenMP threads, but can be overcome by the use of dynamic scheduling of the computation performed by each thread.5. Discussion The results of the ARB simulations show the formation of a texture gradient in the thickness of the sheet, after both rolling passes. Although no experimental investigations were performed in the current work, the simulation results are seemingly consistent with experimental results of ARB processed aluminum alloy available in the literature. Saito et al. [2] identify a surface shear texture and a rolling texture in the bulk of AA1100 sheets after eight ARB cycles. A texture gradient has also been observed in AA1100 (6 ARB cycles) [76] and in AA1070 (1,2,4 & 6 ARB cycles) [77]. Indeed, the formation of such texture gradients not exclusive to ARB processed alloys and can be seen in conventional rolling processes too, albeit to a lesser degree. A primary reason for this gradient is the deference in the imposed boundary conditions between elements on the surface of the rolled sheet and those at the center. The friction conditions between the roller and the feedstock results in a substantial amount of shear deformation in the elements close to the surface. This superposed shear deformation gradually reduces towards the center of the rolled sheet, a consequence of which, elements close to the center are subjected to almost pure plane strain compression boundary conditions. This is evident in both the predicted texture (cf. g. 4 and fig. 5) and the deformed mesh rolled sheet, as seen in fig. 11 for a central stack of ten elements.

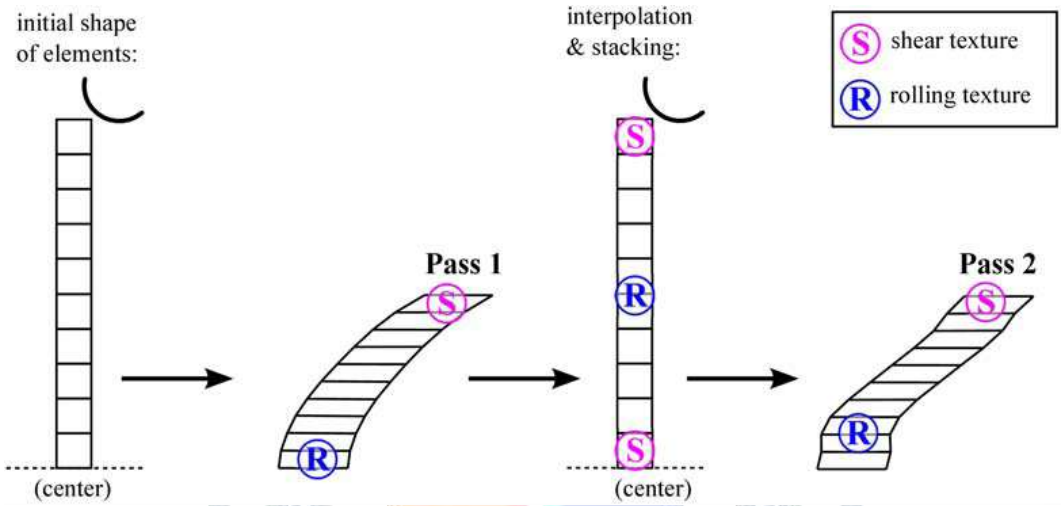

Figure 11: Initial and deformed shapes of the elements in the center cross-section (blue in fig. 1) for ARB cycle 1 and 2, and locations where shear or rolling texture components are most pronounced. After the rolling cycle, texture components are redistributed due to the stacking of sheets. This results in a different through-thickness variation of shear in pass 2.

Since the ARB process involves stacking of two sheets before each pass, the central region of the feed stock(consisting of two sheets) before the second pass now essentially presents a sheer texture. After the second pass, this sheer texture is reduced considerably. Nevertheless, a gradient in texture is still evident, although the center of the top sheet still shows a strong fcc rolling texture.29A direct consequence of the texture gradient in the thickness of the sheet is the differential evolution of the yield surfaces, as seen in fig. 9. We take a closer look at the yield surfaces of two elements, one corresponding to the surface, and the other corresponding to the center of the ARB sheet. Fig. 12 shows the yield surfaces in these two elements after the second pass. For comparison, the yield contours of the classical Tresca [78] and von Mises [79] criteria are also plotted. The yield surfaces have been normalized using 11, in order to facilitate the comparison of shapes of the yield surfaces. The initial random texture of both elements results from effectively in a yield locus that is close to the von Mises criterion. At the end of the second pass, however, there is a discernible difference between the yield surfaces of the two elements. The yield locus of the surface element is highly anisotropic which can be attributed to the shear (accumulated with increasing number of passes) caused by the friction between the roller and the sheet. In comparison, the yield surface of the element close to the center evolves with the lesser amount of anisotropy. Although the two elements in question experience the same amount of shear in the first pass, the element in the center experiences reduced or almost no shear in the second pass, and is dominated by boundary conditions close to plane strain compression. This differential yield behavior is of the significant chance for two additional reasons. First, this behavior is different from what can be expected in multiple pass direct rolling simulations. Or in other words, the anisotropic evolution of the yield surfaces is a direct consequence of the stacking of sheets in the ARB process. Second, engineers aiming to simulate further processes like deep drawing to determine component behavior and reliability must account for this through thickness gradient of the material properties; neglecting it may result in the incorrect estimation of the stress and strain state in the simulations. The proposed modeling framework successfully captures key elements of the ARB process, namely rolling process along with the large thickness reduction, and the evolving texture and anisotropy. It also circumvents mesh deterioration problems in multiple pass rolling. However, in the present form, the framework does not yet include two further important aspects of the ARB process -interlayer bonding strength and their need of grain size leading to UFG microstructure after multiple rolling passes. The modeling framework can, however, be easily extended to include additional features, like e.g. cohesive zone elements, to account for interlayer bonding. The VPSC model embedded in the current framework uses a phenomenological description of the strain rate. This is clearly not sufficient to account for the complex deformation mechanisms and their temperature and strain rate dependence, which is of particular importance in UFG materials. A more physics-based constitutive description is hence necessary to capture intricate details of the mechanics at the small length scales, including activation barriers [80], dislocation-defect interactions [81, 82], grain boundary mediated plasticity [83, 84, 85], amongst others. These are aspects of current development involving physics based constitutive models (e.g. [86, 87, 88], see Ref. [25] for a detailed review of such models). The VPSC model Likewise, constitutive models for grain refinement (e.g. [90]) can

also be easily incorporated in the current framework to account for the UFG microstructure. Even with its current limitations, the present multiscale modeling framework is expected to signify can't contribute to the establishment of the ARB process as an elegant way to produce metal sheets with tailored properties.

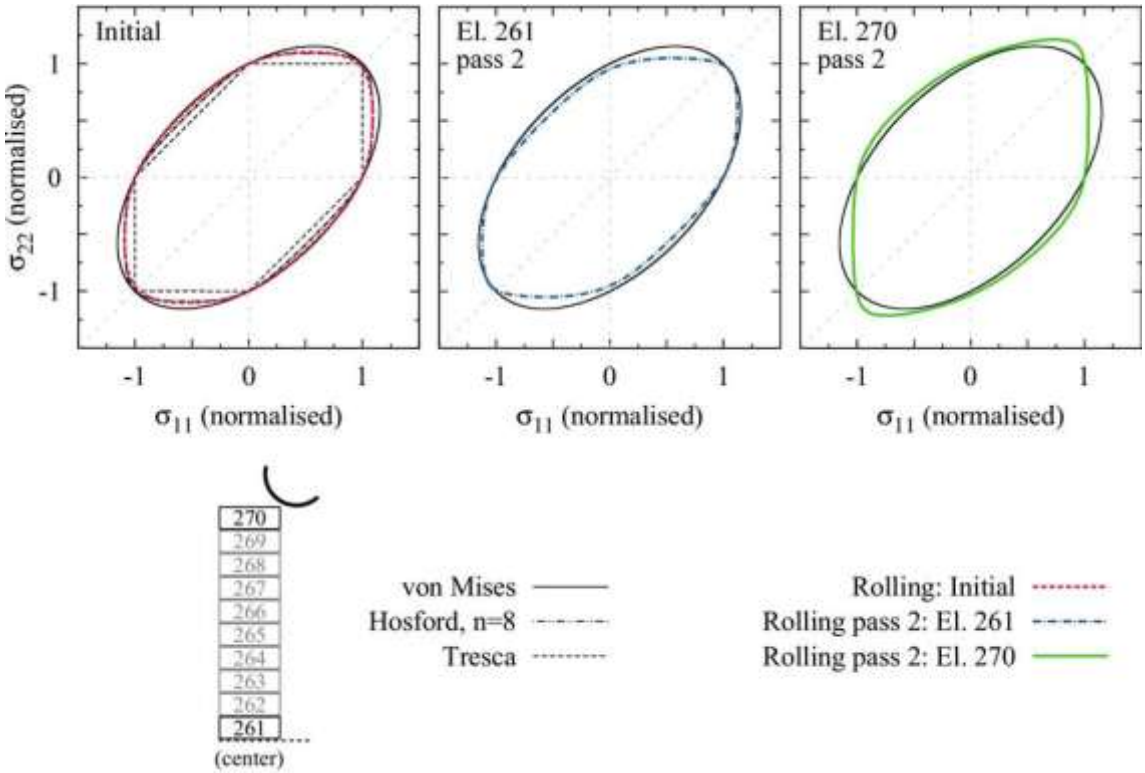

Figure 12: Normalized polycrystalline yield surfaces of the initial state and in elements 261 and 270 after pass 2. The isotropic yield stresses according to the criteria of Tresca [78] and von Mises [79] are also included. Comparison shows that the yield stress is anisotropic after ARB pass 2. The anisotropy is more pronounced in case of the surface element 270.can be directly extended to include such physics based constitutive approaches [89].

The framework can, for instance, be used to optimize processing parameters and conditions required for ARB. Having a reliable and robust simulation framework, which is simultaneously efficient as to provide results in realistic time schedules, can help in up scaling the process to produce sheets of large dimensions required for industrial usage. Furthermore, it can also be used for subsequent forming processes like deep drawing, thereby enabling the simulation of a process chain

V. Conclusions

In this work, we have developed a computational framework that facilitates the simulation of multiple-pass ARB process. To this end, we embed the VPSC model as a VUMAT in the explicit FE formulation of Abaqus. As a result of the evolution of texture during the process, and consequently, the evolving anisotropy is seamlessly accounted for in the framework, and have a direct influence on the processing conditions, like . rolling forces. The main aspects of our framework are as follows: To facilitate the simulation of multiple passes, we propose and implement a novel solution mapping scheme. This scheme essentially maps the texture, grain shapes and other relevant material states variables from the deformed mesh onto a new undistorted mesh. As a result, simulation of the subsequent pass can be done with a mesh of good quality whilst retain the requisite solution variables of the previous pass. This has an additional advantage of circumventing the problem associated with the increase in the number of finite elements with increasing number of ARB passes since the number of the element remains constant with the usage of the solution mapping scheme. The framework implements multi-level parallelization of the material response -decomposition of the nite element domain using MPI and parallelization of the material response using OpenMP threads-resulting in reduced simulation times. Acceleration techniques are made use of in the computational framework to keep simulation times to a minimum. We interrogate the polycrystal model only when certain criteria are met; else a linear stress update using the elastic self-consistent moduli is performed. To the best of our knowledge, the proposed solution mapping scheme and multi-level parallelization entirely new and has hitherto not been presented in the literature. We have demonstrated the computational32framework by simulating a two-pass ARB process. The results clearly show a through thickness gradient of texture and evolving anisotropy, which is a direct consequence of the stacking of sheets. The current computational framework can serve as an important tool that facilitates the incorporation of the ARB process in industry -the framework incorporates a robust and reliable material model, and the two-level parallelization helps realize simulations in realistic time schedules. Finally, we point out that the current framework is not limited to the ARB process. It can be used for the simulation of other forming processes, including conventional rolling, deep drawing etc.

VI. ACKNOWLEDGEMENTS

The authors would like to thank Dr. Surender Kumar Precedent of Indo-US research institute for sustainable development , and Prof. P.B. Sharma Vice Chancellor Amity University Haryana Gurgaon, for fruitful discussions.

REFERENCES

[1] N. R. C. Committee on Integrated Computational Materials Engineering, Integrated computational materials Engineering: A Transformational Discipline for Improved Competitiveness and National Security, The National Academies Press, 2008.

[2] Y. Saito, N. Tsuji, H. Utsunomiya, T. Sakai, R. Hong, Scripta Materialia 39 (1998) 1221-1227.
[3] N. Tsuji, Nanostructured metals and alloys, Woodhead Publishing, Philadelphia, 2011, Ch. 2: Bulk nanostructured metals and alloys produced by accumulative roll-bonding, pp. 40-57.
[4] M. Ruppert, W. Bohm, H. Nguyen, H. W. Hoppel, M. Merklein, M. Goken, Journal of Materials Science48 (2013) 8377-8385.
[5] M. Goken, H. W. Hoppel, Advanced Materials 23 (2011) 2663-2668.
[6] T. Hausol, V. Maier, C. W. Schmidt, M. Winkler, H. W. Hoppel, M. Goken, Advanced EngineeringMaterials 12 (2010a) 740-746.
[7] S. Roy, B. R. Nataraj, S. Suwas, S. Kumar, K. Chattopadhyay, Journal of Materials Science 47 (2012)6402-6419.
[8] T. Hausol, H. W. Hoppel, M. Goken, Journal of Materials Science 45 (2010) 4733-4738.33
[9] C. W. Schmidt, P. Knodler, H. W. Hoppel, M. Goken, Metals 1 (1) (2011) 65-78. doi:10.3390/met1010065.
[10] C. W. Schmidt, M. Ruppert, H. W. Hoppel, F. Nachtrab, A. Dietrich, R. Hanke, M. Goken, Advanced Engineering Materials 14 (2012) 1009-1017.
[11] R. Jamaati, M. R. Toroghinejad, Materials Science and Engineering, A 527 (27) (2010) 7430-7435.
[12] R. Jamaati, M. R. Toroghinejad, Materials Science, and Engineering: A 527 (16) (2010) 4146-4151.
[13] M. Alizadeh, M. H. Paydar, Journal of Alloys and Compounds 492 (2010) 231-235.
[14] N. Tsuji, Y. Saito, H. Lee, Y. Minamino, Advanced Engineering Materials 5 (2003) 338-344.
[15] H. Hoppel, J. May, M. Goken, Advanced Engineering Materials 6 (2004) 781-784.
[16] R. Z. Valiev, I. V. Alexandrov, Y. T. Zhu, T. C. Lowe, Journal of Materials Research 17 (2002) 5-8.doi:10.1557/JMR.2002.0002.
[17] B. Beausir, J. Scharnweber, J. Jaschinski, H.-G. Brokmeier, C.-G. Oertel, W. Skrotzki, Material Science and Engineering A 527 (2010) 3271-3278.
[18] X. Huang, N. Tsuji, N. Hansen, Y. Minamino, Materials Science and Engineering: A 340 (2003) 265 -271.
[19] C. Heason, P. Prangnell, Materials Science Forum 408-412 (2002) 733-738.
[20] G. I. Taylor, Journal of the Institute of Metals 62 (1938) 307-327.
[21] H. Pirgazi, A. Akbarzadeh, R. Petrov, J. Sidor, L. Kestens, Materials Science and Engineering A 492(2008) 110-117.
[22] P. Van Houtte, A. K. Kanjarla, A. V. Bael, M. Seefeldt, L. Delannay, European Journal of MechanicsA/Solids 25 (2006) 634-648.
[23] S. Li, F. Sun, H. Li, Acta Materialia 58 (2010) 1317-1331.
[24] T. Inoue, N. Tsuji, Computational Materials Science 46 (2009) 261-266.
[25] F. Rogers, P. Eisenlohr, L. Hantcherli, D. Tjahjanto, T. Bieler, D. Raabe, Acta Materialia 58 (2010)1152-1211.
[26] A. Prakash, Computational micromechanics of polycrystals: Special emphasis on twinning and recrystallization in Mg alloys and TWIP steels, Ph.D. thesis, Karlsruhe Institute of Technology (2010).34
[27] F. Barbe, L. Decker, D. Jeulin, G. Cailletaud, International Journal of Plasticity 17 (2001) 513-536.
[28] O. Dillard, S. Leclercq, G. Rousselier, G. Cailletaud, International Journal of Plasticity 21 (2005) 691-722.
[29] A. Prakash, S. M. Weygand, H. Riedel, Computational Materials Science 45 (2009) 744-750. doi:doi:10.1016/j.commatsci.2008.06.015.
[30] D. Raabe, M. Sachtleber, Z. Zhao, F. Roters, S. Zae
erer, Acta Materialia 49 (2001) 3433-3441.
[31] A. Bhattacharyya, E. El-Danaf, S. Kalidindi, R. Doherty, International Journal of Plasticity 17 (2001)861-883.
[32] B. Klusemann, B. Svendsen, H. Veho
, Computational Materials Science 52 (1) (2012) 25 -32, Proceedings of the 20th International Workshop on Computational Mechanics of Materials - fIWCMMg20. doi:http://dx.doi.org/10.1016/j.commatsci.2011.03.042.
[33] R. A. Lebensohn, Acta Materialia 49 (2001) 2723-2737.
[34] P. Eisenlohr, M. Diehl, R. Lebensohn, F. Roters, International Journal of Plasticity 46 (2013) 37-53.
[35] A. Prakash, R. A. Lebensohn, Modelling and Simulation in Materials Science and Engineering 17 (2009)064010. doi:10.1088/0965-0393/17/6/064010.
[36] F. Feyel, Computer Methods in Applied Mechanics and Engineering 183 (2003) 309-330.
[37] P. Van Houtte, S. Yerra, A. Van Bael, International Journal of Plasticity 25 (2009) 332-360.
[38] W. He, S. Zhang, A. Prakash, D. Helm, Computational Materials Science 82 (2014) 464-475.
[39] R. Hill, International Journal of Mechanical Sciences 35 (1993) 19-25.
[40] F. Barlat, J. Yoon, O. Cazacu, International Journal of Plasticity 23 (2007) 876-896.
[41] N. Barton, J. Knap, A. Arsenlis, R. Becker, R. Hornung, D. Je
fferson, International Journal of Plasticity24 (2008) 242-266.
[42] R. Lebensohn, C. Tome, Acta Metallurgica et Materialia 41 (1993) 2611-2624.
[43] A. Prakash, T. Hochrainer, E. Reisacher, H. Riedel, Steel Research International 79(8) (2008) 645-652.doi:DOI:10.2374/SRI08SP030-79-2008-645.
[44] T. Walde, H. Riedel, Acta Materialia 55 (2007) 867-874.
[45] G. C. Kaschner, J. F. Bingert, C. Liu, M. L. Lovato, P. J. Maudlin, M. G. Stout, C. N. Tome, ActaMaterialia 49 (2001) 3097-3108.35
[46] A. Prakash, C. Schmidt, H. Riedel, R. Kawalla, Experimental and Numerical Investigation of the activation of Pyramidal Slip during Deformation of Cast-Rolled Magnesium alloy AZ31, in: Proc. 8thMagnesium Conf., Weimar, Germany, 2009a.
[47] S. R. Agnew, M. H. Yoo, C. N. Tome, Acta Materialia 49 (2001) 4277-4289.
[48] C. N. Tome, P. J. Maudlin, R. A. Lebensohn, G. C. Kaschner, Acta Materialia 49 (2001) 3085-3096.
[49] J. Segurado, R. A. Lebensohn, J. Llorca, C. Tome, International Journal of Plasticity 28 (2012) 124-140.
[50] M. Knezevic, R. J. McCabe, R. A. Lebensohn, C. N. Tome, C. Liu, M. L. Lovato, B. Mihaila, Journal of the Mechanics and Physics of Solids 61 (2013) 2034-2046.
[51] R. Chandra, L. Dagum, D. Kohr, D. Maydan, J. McDonald, R. Menon, Parallel Programming in OpenMP, Morgan Kaufmann Publishers, 2001.
[52] J. Eshelby, Proceedings of the Royal Society A 241 (1957) 376-396.
[53] R. J. Asaro, Journal of Applied Mechanics 50 (1983) 921-934.
[54] R. J. Asaro, Advances in Applied Mechanics 23 (1983) 1-115.
[55] J. Hutchinson, Proceedings of the Royal Society A 348 (1976) 101-127.
[56] T. Mura, Micromechanics of defects in solids, Martinus Nijho

Publishers, The Hague, The Netherlands,1982.
[57] A. Molinari, G. Canova, S. Ahzi, Acta Metallurgica 35 (1987) 2983-2994.
[58] C. N. Tome, Modelling and Simulation in Materials Science and Engineering 7 (5) (1999) 723.
[59] R. A. Lebensohn, C. N. Tome, P. Ponte Casta~neda, Philosophical Magazine 87 (2007) 4287-4322.
[60] C. Tome, G. Canova, U. Kocks, N. Christodoulou, J. Jonas, Acta Metallurgica 32 (1984) 1637-1653.
[61] E. Voce, Journal of the Institute of Metals 74 (1948) 537-562.
[62] F. J. Harewood, P. E. McHugh, Computational Materials Science 39 (2007) 481-494.
[63] T. Walde, H. Riedel, Solid State Phenomena 105 (2005) 285-290.
[64] T. Walde, International Journal of Refractory Metals and Hard Materials 26 (2008) 396-403.
[65] Abaqus Inc., Abaqus/Explicit: Advanced Topics -Appendix 3: Writing a VUMAT, Workshop (2005).
[66] S. Mercier, A. Molinari, International Journal of Plasticity 25 (2009) 1024-1048.36
[67] H. Wang, P. Wu, C. Tome, Y. Huang, Journal of the Mechanics and Physics of Solids 58 (2010) 594-612.
[68] H.-J. Bunge, Texture Analysis in Materials Science: Mathematical Methods, Cuvillier Verlag, G□Gottingen,1999.
[69] K. Shoemake, Animating rotation with quaternion curves, in: SIGGRAPH'85 Proceedings of the 12thannual conference on Computer graphics and interactive techniques, 1985, pp. 245-254.
[70] A. Morawiec, J. Pospiech, Textures and Microstructures 10 (1989) 211-216.
[71] C. N. Tome, R. A. Lebensohn, Manual for VPSC -version 7 (2009).
[72] W. G. N□Dohring, Towards a nite element multiscale model of the accumulative roll bonding process, Master's thesis, Friedrich-Alexander-Universit□at Erlangen-Nurnberg (2013).
[73] W. G. N□Dohring, A. Prakash, E. Bitzek, In preparation.
[74] C. N. Tome, R. A. Lebensohn, C. T. Necker, Metallurgical and Materials Transactions A 33 (2002)2635-2648.
[75] F. Bachmann, R. Hielscher, H. Schaeben, Solid State Phenomena 160 (2010) 63-68. doi:10.4028/www.scientific.net/SSP.160.63.
[76] C. Heason, P. Prangnell, Materials Science Forum 408-412 (2002) 733-738.
[77] S. Li, F. Sun, H. Li, Acta Materialia 58 (2010) 1317-1331.
[78] H. Tresca, Comptes Rendus Hebdomadaires de l'Academie des Sciences Paris 59 (1864) 754-758.
[79] R. von Mises, Nachrichten der Akademie der Wissenschaften zu G□ottingen, Mathematisch-PhysikalischeKlasse 1 (1913) 582-592.
[80] Y. Fan, Y. N. Osetskiy, S. Yip, B. Yildiz, Proceedings of the National Academy of Sciences 110 (44)(2013) 17756-17761. doi:10.1073/pnas.1310036110.
[81] E. Bitzek, P. Gumbsch, Materials Science and Engineering: A 387 (2004) 11-15.
[82] E. Bitzek, P. Gumbsch, Materials Science and Engineering: A 400 (2005) 40-44.
[83] Y. Wei, L. Anand, Journal of the Mechanics and Physics of Solids 52 (11) (2004) 2587 -2616. doi:http://dx.doi.org/10.1016/j.jmps.2004.04.006.
[84] D. Gianola, S. V. Petegem, M. Legros, S. Brandstetter, H. V. Swygenhoven, K. Hemker, Acta Materialia54 (8) (2006) 2253 -2263. doi:http://dx.doi.org/10.1016/j.actamat.2006.01.023.37
[85] F. Mompiou, D. Caillard, M. Legros, Acta Materialia 57 (7) (2009) 2198 -2209. doi:http://dx.doi.org/10.1016/j.actamat.2009.01.014.
[86] M. Meyers, D. Benson, O. V□ohringer, B. Kad, Q. Xue, H.-H. Fu, Materials Science and Engineering: A322 (1-2) (2002) 194 -216. doi:http://dx.doi.org/10.1016/S0921-5093(01)01131-5.
[87] R. A. Austin, D. L. McDowell, International Journal of Plasticity 27 (1) (2011) 1 -24. doi:http://dx.doi.org/10.1016/j.ijplas.2010.03.002.
[88] H. Lim, L. Hale, J. Zimmerman, C. Battaile, C. Weinberger, International Journal of Plasticity (xx)(2015) -. doi:http://dx.doi.org/10.1016/j.ijplas.2014.12.005.
[89] H. Wang, P. Wu, C. Tome, J. Wang, Materials Science and Engineering: A 555 (0) (2012) 93 -98.doi:http://dx.doi.org/10.1016/j.msea.2012.06.038.
[90] I. Beyerlein, R. Lebensohn, C. Tome, Materials Science and Engineering A 345 (2003) 122-138.38
[91] S.Sharma, R. P. Singh, S. Kumar, Indian Journal of Science and Technology: 345 (2016) 2-7